negligible. Thus the fundamental dissipation process remains the same and we expect the turbulence to be qualitatively unaffected by the Pr shift. In the He experiments the Pr shift is from 0.7 to 7 with the result that the primary dissipation mechanism shifts from thermal diffusion to viscous damping, for different locations within the same cell at a single Ra number.

In Hg, in which these complicating factors do not contribute (and for substantially higher Re), we see no evidence of a transition. Thus ultrahard turbulence may not exist. □

Received 17 July; accepted 29 December 1998.

1. Shraiman, B. I. & Siggia, E. D. Heat transport in high-Rayleigh-number convection. *Phys. Rev. A* **42,** 3650–3653 (1990).
2. Siggia, E. D. High Rayleigh number convection. *Annu. Rev. Fluid Mech.* **26,** 137–168 (1994).
3. Kraichnan, R. H. Turbulent thermal convection at arbitrary Prandtl number. *Phys. Fluids* **5,** 1374–1389 (1962).
4. Howard, L. N. Bounds on flow quantities. *Annu. Rev. Fluid Mech.* **4,** 473–494 (1972).
5. Busse, F. H. The optimum theory of turbulence. *Adv. Appl. Mech.* **18,** 77–121 (1978).
6. Castaing, B. *et al.* Scaling of hard thermal turbulence in Rayleigh-Bénard convection. *J. Fluid Mech.* **204,** 1–30 (1989).
7. Cioni, S., Ciliberto, S. & Sommeria, J. Strongly turbulent Rayleigh–Bénard convection in mercury: comparison with results at moderate Prandtl number. *J. Fluid Mech.* **335,** 111–140 (1997).
8. Chavanne, X. *et al.* Observation of the ultimate regime in Rayleigh–Bénard convection. *Phys. Rev. Lett.* **79,** 3648–3651 (1997).
9. Belmonte, A., Tilgner, A. & Libchaber, A. Temperature and velocity boundary layers in turbulent convection. *Phys. Rev. E* **50,** 269–279 (1994).
10. Segawa, T., Naert, A. & Sano, M. Matched boundary layers in turbulent Rayleigh–Bérnard convection of mercury. *Phys. Rev. E* **57,** 557–560 (1998).
11. Wu, X. Z. & Libchaber, A. Scaling relations in thermal turbulence: The aspect-ratio dependence. *Phys. Rev. A* **45,** 842–845 (1992).
12. Schewe, P. F. & Stein, B. One of the most convective fluids observed in the laboratory. *Physics News Update 342-1* (Am. Inst. Phys., 1997).
13. Heslot, F., Castaing, B. & Libchaber, A. Transition to turbulence in helium gas. *Phys. Rev. A* **36,** 5870–5873 (1987).
14. Wu, X. Z., Kadanoff, L., Libchaber, A. & Sano, M. Frequency power spectrum of temperature fluctuations in free convection. *Phys. Rev. Lett.* **64,** 2140–2143 (1990).
15. Wu, X. Z. & Libchaber, A. Non-Boussinesq effects in free thermal convection. *Phys. Rev. A* **43,** 2833–2839 (1991).
16. Takeshita,, T., Segawa, T., Glazier, J. A. & Sano, M. Thermal turbulence in mercury. *Phys. Rev. Lett.* **76,** 1465–1468 (1995).
17. Naert, A., Segawa, T. & Sano, M. High-Reynolds-number thermal turbulence in mercury. *Phys. Rev. E* **56,** 1302–1305 (1997).

Acknowledgements. J.A.G. was supported by the NSF and the ACS/PRF; M.S. acknowledges support from the Japanese Grant-in-Aid for Science Fund for the Ministry of Education, Science and Culture. Both are supported by the NSF-JSPS Cooperative Science Program.

Correspondence and requests for materials should be addressed to J.A.G. (e-mail: jglazier@rameau.phys.nd.edu).

Picosecond–milliångström lattice dynamics measured by ultrafast X-ray diffraction

Christoph Rose-Petruck*†, Ralph Jimenez*†, Ting Guo*, Andrea Cavalleri*, Craig W. Siders*, Ferenc Ráksi*†, Jeff A. Squier§, Barry C. Walker*†, Kent R. Wilson* & Christopher P. J. Barty‡

** Department of Chemistry and Biochemistry, ‡ The Institute for Nonlinear Science, § Department of Electrical and Computer Engineering, The University of California, San Diego, La Jolla, California 92093–0339, USA*

Fundamental processes on the molecular level, such as vibrations and rotations in single molecules, liquids or crystal lattices and the breaking and formation of chemical bonds, occur on time-scales of femtoseconds to picoseconds. The electronic changes associated with such processes can be monitored in a time-resolved manner by ultrafast optical spectroscopic techniques[1], but the accompanying structural rearrangements have proved more difficult to observe. Time-resolved X-ray diffraction has the potential to probe fast, atomic-scale motions[2–5]. This is made possible by the generation of ultrashort X-ray pulses[6–10], and several X-ray studies of fast dynamics have been reported[6–8,11–15]. Here we report the direct observation of coherent acoustic phonon propagation in crystalline gallium arsenide using a non-thermal, ultrafast-laser-driven plasma—a high-brightness, laboratory-scale source of subpicosecond X-ray pulses[16–19]. We are able to follow a 100-ps coherent acoustic pulse, generated through optical excitation of the crystal surface, as it propagates through the X-ray penetration depth. The time-resolved diffraction data are in excellent agreement with theoretical predictions for coherent phonon excitation[20] in solids, demonstrating that it is possible to obtain quantitative information on atomic motions in bulk media during picosecond-scale lattice dynamics.

Crystalline gallium arsenide (GaAs) is available in large samples of very high crystalline quality, making it an ideal system for quantitative investigations using optical pumping and X-ray probing. Its physical parameters are known with great precision[21], and numerous prior studies[22] on its ultrafast electronic properties provide a solid foundation for interpretation, and for testing the potential of ultrafast X-ray diffraction. Indeed, some information on ultrafast lattice dynamics after optical excitation has already been indirectly inferred from a variety of linear and nonlinear optical techniques[22–24]. But owing to the short penetration depth of visible light, information on bulk dynamics in absorbing materials has not yet been obtained.

Figure 1 shows a schematic of our experiment. An ultrashort pulse of laser-generated Cu Kα X-rays (consisting of two closely spaced lines, $K\alpha_1$ and $K\alpha_2$) diffracts in a symmetric Bragg configuration from the 3.26-Å (111) lattice spacing in GaAs, penetrating ~2 μm into the bulk along the surface normal. A 30-fs pump pulse with variable time delay generates electron–hole pairs via interband excitation within the submicrometre penetration depth of the 800-nm light. By illuminating with light only a portion of the area probed by X-rays, we simultaneously observe the Kα lines from both photopumped and unperturbed areas of the semiconductor surface. Two-minute exposure X-ray-CCD images are normalized with respect to the incident X-ray flux and binned within the region of uniform illumination. In Fig. 2, the measured and calculated (described below) diffraction profiles are shown as a function of angular deviation from the Bragg angle, $\theta - \theta_B$, and of pump–probe time delay. Zero delay corresponds to the initial deviation of the diffracted signal. We observe for these early times that both of the original Kα lines broaden and shift slightly to larger angles (~20 arcsec), while two new lines appear, broader and weaker than the original lines and deviate by approximately −150 arcsec relative to the original Bragg angle. As the pump–probe delay is increased, these new lines decrease in width, increase in intensity, and merge asymptotically with the still broadened and shifted main lines. Finally, the angle-integrated diffraction signal (not shown) increases monotonically with delay, reaching a plateau of twice the unperturbed value.

The incident optical energy couples into the material by promoting electrons from the valence to the conduction band. Single- and two-photon (as well as free-carrier) absorption contribute to excitation during absorption of the pump pulse. Bandgap renormalization and state filling, not well characterized at these fluences, introduce additional nonlinearities to the excitation process. Also, efficient carrier diffusion at early times may smooth the energy deposition profile in a few picoseconds. After absorption, energy is transferred to the lattice via intraband relaxation[22] and delayed Auger heating[25]. Existing estimates of the Auger coefficient[26] in GaAs indicate that most of the energy is efficiently transferred to the lattice within a few picoseconds. X-ray diffraction, primarily sensitive to the acoustic phonon population, occurs only after the decay of the initially generated longitudinal optical phonons[22]. Following

† Present addresses: Department of Chemistry, Brown University, Providence, Rhode Island, USA (C.R.-P.); The Scripps Research Institute, La Jolla, California, USA (R.J.); IMRA America, Ann Arbor, Michigan, USA (F.R.); Department of Physics and Astronomy, the University of Delaware, Newark, Delaware, USA (B.C.W.).

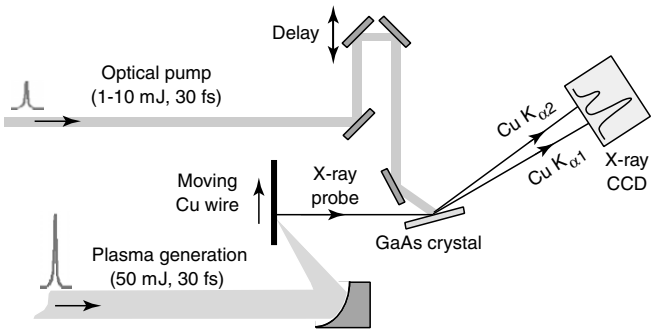

Figure 1 Diagram of the table-top ultrafast X-ray diffractometer. The 800-nm laser pulses are generated at 20 Hz by an ultrafast Ti:sapphire laser producing 30-fs pulses of 200-mJ energy[30]. The output of the laser is used for both sample excitation and X-ray generation. The latter is done by focusing 30-fs, 50-mJ, laser pulses onto a moving Cu wire in vacuum, resulting in a source with measured diameter of ~25 μm. With an average laser power of 1.0 W, $\sim 5 \times 10^{10}$ Cu Kα photons (4π sr s^{-1}) are produced. The emitted Kα radiation–which consists of two closely spaced, $K\alpha_1$ (1.5407 Å) and $K\alpha_2$ (1.5439 Å), lines–is diffracted from the optically pumped GaAs and detected by an X-ray CCD camera, with a data acquisition time of two minutes per delay step. We excite the GaAs crystal with ~30-fs pulses at a fluence of 59 mJ cm^{-2}. The flat-top pump beam size is set to ~4 mm^2 (95 ± 5% of peak) so that it includes the sample area encompassing the Bragg angles of the two Kα lines and the auxiliary lines. The crystal is continuously moved during the experiment in order to minimize the effects of cumulative damage by the optical pump pulse.

our line of interpretation and the available parameters, we calculate a ~300-nm thermal energy deposition length, with a maximum surface temperature increase of ~800 K after 10 ps. Therefore, the efficient transfer of incident optical energy to lattice thermal energy can be considered complete after ~10 ps.

Subsequent lattice dynamics and related propagation effects are interpreted as proposed by Thomsen *et al.*[20], who solved the elastic equations assuming impulsively generated thermal stress in an absorbing solid. Stress is relieved by lattice expansion that necessarily starts at the crystal surface, with Newton's third law subsequently driving a travelling compression/expansion strain wave into the bulk at the longitudinal speed of sound ($v_L = 5{,}397$ m s^{-1} in (111)-GaAs[21]). Hence, mechanical relaxation of an impulsively stressed lattice layer of thickness d occurs within a time span of dv_L^{-1}, which corresponds to ~300 ps for our X-ray probe depth. As both energy deposition and probing occur significantly faster than mechanical relaxation, this is a regime where the generation and observation of coherent lattice dynamics is possible. This contrasts with many prior experiments[6,13], where laser heating is slower than mechanical relaxation and the strain is linearly proportional to the temperature. We note that for our experiment, a fully thermo-elastic treatment with coherent phonon excitation must be applied.

We numerically solve the thermo-elastic problem using the known parameters[21] for GaAs, together with the calculated energy deposition depth and temperature rise (Fig. 3). Only three parameters are used in the model: the peak strain which is obtained directly from the data, the acoustic velocity which is known from the literature[21], and the absorption length, ζ, which we estimate to be 300 nm. We systematically varied ζ within its uncertainty (±30%); 275 nm gave the best fit to the data. The calculated temperature increase corresponds to a maximum surface strain of ~0.25%, or 8 mÅ of lattice expansion, after the stress is released, which is in good agreement with the experimental 150-arcsec deviation seen near zero delay in Fig. 2a. However, our data cannot exclude additional non-thermal strain generation[20] from the hot, dense electron–hole plasma at early times. A 100-ps acoustic pulse propagates into the crystal at v_L and has peak bipolar strain of approximately ±0.12%, or ±3 mÅ. The theoretical time-resolved diffraction curves of Fig. 2b, corresponding to the strain profile in Fig. 3, were calculated using standard Takagi–Taupin[27–29] techniques and convolved with the spectral and spatial distributions of our X-ray source. They are in good agreement with the experimental data of Fig. 2a. Inclusion of thermal diffusion[20] into the elastic equations effected higher-order dispersive strain behaviour, but, to within our experimental resolution, produces insignificant changes to the calculated diffraction profiles.

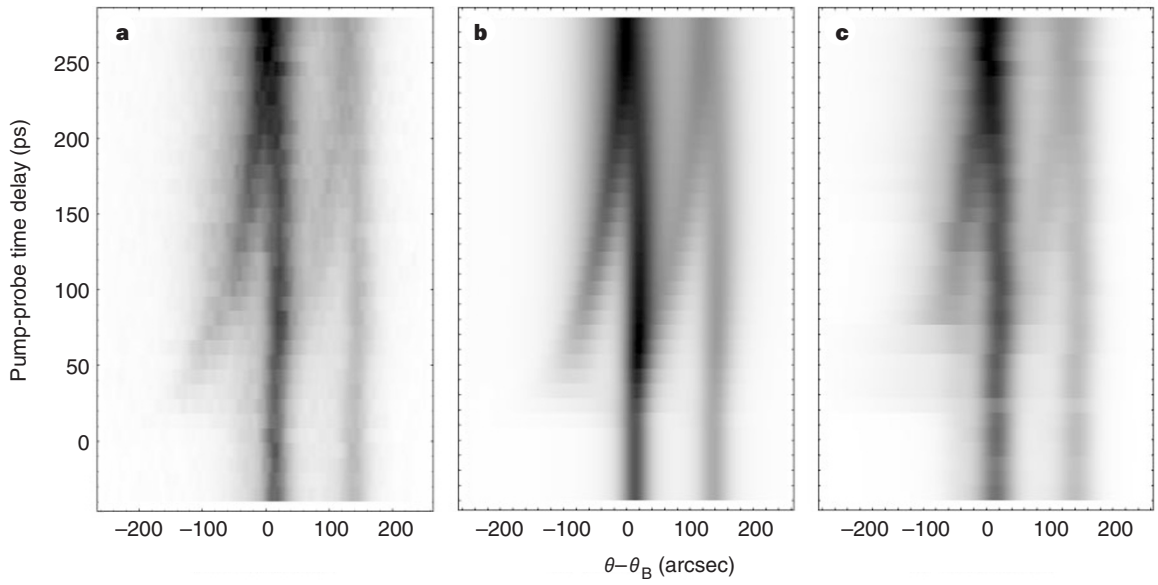

Figure 2 Experimentally measured (**a**), theoretically calculated (**b**), and iteratively inverted (**c**) time- and angle-resolved diffraction curves for optically excited GaAs. The horizontal axis is angular deviation from the $K\alpha_1$ Bragg angle calculated assuming unit refractive index. Vertical axis is pump–probe time delay, with the zero of delay being chosen to coincide with the initial deviation of the lines from their unpumped appearance. For **c**, the iterative genetic-algorithm inversion procedure varied the depth-dependent strain, defined by a 200-nm-spaced, cubic-spline-interpolated grid, and calculated the corresponding diffraction patterns until a good fit was achieved. Five inversions with different parameters of the genetic algorithm, such as random number seed, population size, crossover probability, and mutation rate, were performed and subsequently averaged.

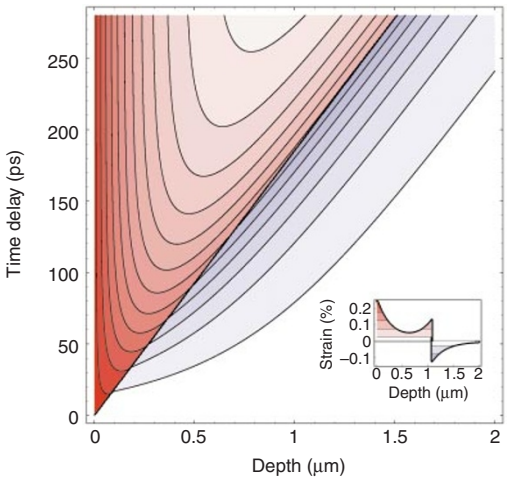

Figure 3 Theoretically calculated percentage lattice expansion, or strain, within the GaAs crystal as a function of depth and pump–probe time delay. Inset, the depth-dependent strain at a pump–probe delay of 200 ps. As indicated in the inset, regions of lattice expansion are indicated with an increasingly strong red, while regions of lattice compression are indicated similarly in blue. The white region indicates zero strain, that is, the unpumped lattice spacing. Contours are drawn at intervals of 0.02% of the static lattice plane spacing ($d_0 = 3.26$ Å), with the peak strain at the surface corresponding to 0.25%, that is 8.2 mÅ of lattice expansion. The prominent red and blue diagonal represents the elastic strain wave, which starts at the surface and propagates, with compression leading expansion, into the bulk at 5,397 m s^{-1}.

Comparing Figs 2a, b and 3, we see that the initially thin but highly strained layer of lattice expansion produces the broad, low-intensity lines at early time delays. As the strain wave propagates away from the surface, the layer of surface expansion thickens and these lines correspondingly become narrower and more intense, but diffract at smaller angular deviations due to the weaker average strain. In parallel, the compression wave leading the propagation into the bulk contributes to the slight shift to higher angles seen in the main Kα lines. At the longest delays, the strain wave has largely moved beyond the depths probed by the X-ray pulse, and we see diffraction lines broadened and shifted slightly to lower angles due to the exponential surface strain of the relaxed lattice. The strain for these late times is simply proportional to the temperature distribution. Finally, the theoretical angle-integrated diffraction signal similarly reproduces the monotonic increase and plateau behaviour seen in the experimental data.

Additionally, we performed an iterative genetic-algorithm inversion, obtaining the strain from the measured data. The angle- and time-resolved diffraction curves corresponding to the retrieved strain are shown in Fig. 2c. Spectral and geometrical broadening of the diffraction lines significantly limits the uniqueness of the result. Nevertheless, we obtain qualitatively similar strain behaviour to that shown in Fig. 3. We retrieve an exponential surface strain, with 8-mÅ peak strain, and a unipolar, 3-mÅ strain pulse which propagates into the bulk at several thousand metres per second. Although the physical model that we used is fully consistent with the measured data (to within our experimental resolution), the spectral and geometrical broadening mentioned above mean that it is not a unique interpretation of that data.

This work, using a table-top laboratory apparatus, demonstrates with a simple crystalline material the direct observation of milli-ångström atomic motion on the picosecond timescale. Further developments of the technique should permit direct observation by ultrafast X-ray diffraction of the ultrafast atomic motions accompanying a wide variety of physical, chemical, and perhaps biological processes. □

Received 21 October 1998; accepted 9 February 1999.

1. Elsaesser, T., Fujimoto, J. G., Wiersma, D. A. & Zinth, W. (eds) *Ultrafast Phenomena XI* (Springer, Berlin, 1998).
2. Rentzepis, P. M. & Helliwell, J. R. (eds) *Time-Resolved Diffraction* (Oxford Univ. Press, 1997).
3. Bergsma, J. P. *et al.* Transient x-ray scattering calculated from molecular dynamics. *J. Chem. Phys.* **84,** 6151–6160 (1986).
4. Wark, J. Time-resolved x-ray diffraction. *Contemp. Phys.* **37,** 205–218 (1996).
5. Ben-Nun, M., Cao, J. S. & Wilson, K. R. Ultrafast x-ray and electron diffraction: Theoretical considerations. *J. Phys. Chem. A* **101,** 8743–8761 (1997).
6. Larson, B. C., Tischler, J. Z. & Mills, D. M. Nanosecond resolution time-resolved x-ray study of silicon during pulsed-laser irradiation. *J. Mater. Res.* **1,** 144–154 (1986).
7. Srajer, V. *et al.* Photolysis of the carbon monoxide complex of myoglobin: nanosecond time-resolved crystallography. *Science* **274,** 1726–1729 (1996).
8. Chen, P., Tomov, I. V. & Rentzepis, P. M. Time resolved heat propagation in gold crystals by means of picosecond x-ray diffraction. *J. Chem. Phys.* **104,** 10001–10007 (1996).
9. Schoenlein, R. W. *et al.* Femtosecond x-ray pulses at 0.4 Å generated by 90 degree Thomson scattering: a tool for probing the structural dynamics of materials. *Science* **274,** 236–238 (1996).
10. Murnane, M. M., Kapteyn, H. C., Rosen, M. D. & Falcone, R. W. Ultrafast x-ray pulses from laser-produced pulses. *Science* **251,** 531–536 (1991).
11. Rischel, C. *et al.* Femtosecond time-resolved X-ray diffraction from laser-heated organic films. *Nature* **390,** 490–492 (1997).
12. Chin, A. H. *et al.* in *Ultrafast Phenomena XI* (eds Elsaesser, T., Fujimoto, J. G., Wiersma, D. A. & Zinth, W.) 401–403 (Springer, Berlin, 1998).
13. Buschert, J. R., Tischler, J. Z., Mills, D. M., Zhao, Q. & Corella, R. Time-resolved x-ray diffraction study of laser annealing in silicon at grazing-incidence. *J. Appl. Phys.* **66,** 3523–3525 (1989).
14. Wark, J. S., Riley, D., Woolsey, N. C., Keihn, G. & Whitlock, R. R. Direct measurement of compressive and tensile strain during shock breakout by use of subnanosecond x-ray diffraction. *J. Appl. Phys.* **68,** 4531–4534 (1990).
15. Larsson, J. *et al.* Ultrafast structural changes measured by time-resolved x-ray diffraction. *Appl. Phys. A* **66,** 587–591 (1998).
16. Kieffer, J.-C. *et al.* Ultrafast x-ray sources. *Phys. Fluids B* **5,** 2676–2681 (1993).
17. Rousse, A. *et al.* Efficient K alpha x-ray source from femtosecond laser-produced plasmas. *Phys. Rev. E* **50,** 2200–2207 (1994).
18. Kmetec, J. D. *et al.* MeV x-ray generation with a femtosecond laser. *Phys. Rev. Lett.* **68,** 1527–1530 (1992).
19. Gallant, P. *et al.* Subpicosecond time-resolved x-ray spectroscopy of plasmas produced by high intensity ultrashort laser pulses. *Proc. SPIE* **3157,** 44–51 (1997).
20. Thomsen, C., Grahn, H. T., Maris, H. J. & Tauc, J. Surface generation and detection of phonons by picosecond light pulses. *Phys. Rev. B* **34,** 4129–4138 (1986).
21. Blakemore, J. S. Semiconducting and other major properties of gallium arsenide. *J. Appl. Phys.* **53,** R123–R181 (1981).
22. Shah, J. *Ultrafast Spectroscopy of Semiconductors and Semiconductor Nanostructures* (Springer, Berlin, 1996).
23. Shank, C. V., Yen, R. & Hirlimann, C. Femtosecond-time-resolved surface structural dynamics of optically excited silicon. *Phys. Rev. Lett.* **51,** 900–902 (1983).
24. Saeta, P., Wang, J.-K., Siegal, Y., Bloembergen, N. & Mazur, E. Ultrafast electronic disordering during the femtosecond laser melting of GaAs. *Phys. Rev. Lett.* **67,** 1023–1026 (1991).
25. Downer, M. C. & Shank, C. V. Ultrafast heating of silicon on sapphire by femtosecond optical pulses. *Phys. Rev. Lett.* **56,** 761–764 (1986).
26. Strauss, U. & Ruhle, W. W. Auger recombination in intrinsic GaAs. *Appl. Phys. Lett.* **62,** 55–57 (1993).
27. Takagi, S. A dynamical theory of diffraction for a distorted crystal. *J. Phys. Soc. Jpn* **26,** 1239–1253 (1969).
28. Taupin, D. Théorie dynamique de la diffraction des rayon X par les cristaux déformés. *Bull. Soc. Fr. Minér. Crist.* **87,** 469–511 (1964).
29. Larson, B. C., White, C. W., Noggle, T. S., Barhost, J. F. & Mills, D. M. Time-resolved x-ray diffraction measurement of the temperature and temperature gradients in silicon during pulsed laser annealing. *Appl. Phys. Lett.* **42,** 282–284 (1983).
30. Barty, C. P. J. *et al.* Generation of 18-fs, multiterawatt pulses using regenerative pulse shaping and chirped pulse amplification. *Opt. Lett.* **21,** 668–670 (1996).

Correspondence and requests for materials should be addressed to K.R.W. (e-mail: krwilson@ucsd.edu).

Directed nucleation of calcite at a crystal-imprinted polymer surface

S. M. D'Souza*, C. Alexander*, S. W. Carr†‡, A. M. Waller§, M. J. Whitcombe* & E. N. Vulfson*

** Institute of Food Research, Earley Gate, Whiteknights Road, Reading RG6 6BZ, UK*

† Unilever Research, Port Sunlight Laboratory, Wirral L63 3JW, UK

§ Unilever Research, Weena 455, 3000DK Rotterdam, Netherlands

The finely tuned properties of natural biominerals and composites reflect the remarkable level of control that is exercised over the size, shape and organization of the constituent crystals[1–4]. Achieving this degree of control over synthetic materials might therefore lead to superior material properties. Organic small molecules, polymers or surfactant mesophases have been used

‡ Present address: ANSTO, Private Mail Bag 1, Mendi 2234, Australia.